Compact remanence-free permanent magnet-based variable magnetic field source

S. Ivanov[(1)]*, H. Chen[(2)], M. Szurek[(1)], and S. Urazhdin[(1)]

[(1)]*Department of Physics, Emory University, Atlanta, Georgia 30322, USA*

[(2)]*Westminster High School, Atlanta, Georgia 30327, USA*

*Corresponding author: sergei.vladimirovich.ivanov@emory.edu

Abstract

We demonstrate a simple and compact variable magnetic field source based on the permanent cube magnet array approximating a Halbach cylinder. The large air gap area accommodates standard cryostat tails while providing a high uniformity and magnetic field stability of up to 0.5 Tesla over regions of up to about a centimeter. It eliminates magnetic remanence effects and produces reproducible fields without the need for feedback. Thanks to the low cost and exceptional energy efficiency, it provides an accessible solution for modest magnetic field requirements in a wide range of research applications.

I. Introduction

Magnetic fields find numerous applications in experimental science and technology ranging from motors and magnetic train levitation to elementary particle studies and determination of fundamental constants via the quantum Hall effect. Yet, the generation of variable magnetic fields beyond a few milliTesla (mT) generally requires large [1], power-hungry [2, 3], and costly electromagnets and current sources, making them inaccessible in many research settings aside from specialized laboratories. Soft iron core electromagnets generally suffer from a significant hysteresis [4], which in the absence of a feedback loop provided by a separate Hall field sensor results in an uncertainty of the generated field, including significant remanent fields in the absence of driving current. Furthermore, the limitations of the current feedback loop in the power supplies can result in substantial magnetic noise that can compromise high-sensitivity measurements. Superconducting electromagnets do not suffer from remnant field problems at the cost of even higher cost and operational complexity.

With the advent of rare earth magnetic materials with a high flux density, permanent magnets became a viable compact, energy-efficient alternative to electromagnets as a source of magnetic fields of up to several Tesla. The field of a single dipole magnet is highly non-uniform and rapidly decreases away from its surface, resulting in safety hazards such as large magnetic forces on the objects in its vicinity. The approach to solving this problem was proposed by Mallinson, who showed that linear permanent magnet arrays with rotating magnetization can confine the field to only one side of the array [5]. Halbach furthered the idea of using permanent magnet arrangements to achieve desirable magnetic field distributions, initially for the quadrupole field commonly used for beam focusing in accelerators [6], and in subsequent work for other magnetic field configurations [7]. In particular, he showed that a suitable permanent magnet arrangement, commonly referred to as the Halbach cylinder, can produce large highly homogeneous fields confined to the desired volume, providing a viable alternative to dipolar electromagnets in applications that do not require magnetic field variation.

Thanks to their versatility and practicality, Halbach arrays have lent themselves to numerous applications ranging from magnetic levitation to accelerators and low-noise magnetic biasing of cryogenic circuits [8-11]. Furthermore, it was shown that two nested coaxial Halbach cylinders can be rotated relative to one another to produce variable magnetic fields [12]. However, this geometry is bulky, technically difficult to implement, and can be mechanically compromised by the large torques on the cylinders due to the edge effects [13]. As a consequence, Halbach arrays have not gained traction as an alternative to dipole electromagnets.

Here, we present a simple, compact, robust, and economically attractive alternative to dipolar electromagnets for variable quasi-uniform field generation over the cylindrical air gap area compatible with the standard 35 mm-diameter cryostat tails. The design uses an array of commercially available cubic rare earth magnets approximating the Halbach cylinder. The array is moved along the cylinder axis to produce a variable field and rotated around the axis to change the direction of the field. This system is capable of producing fields of up to 0.5 Tesla whose uniformity is only slightly compromised by the magnet array offset at intermediate fields. The cost of the system is an order of magnitude smaller than the comparable electromagnet-based sources, making it highly accessible for a variety of research and academic settings.

II. Design and assembly

We now discuss the system design considerations and its assembly. The design is guided by the geometric requirements of the targeted application and the accessibility of the components (especially magnets) while maximizing the achievable field magnitude and uniformity. The cylindrical air gap with a 36 mm diameter is necessary to fit the standard 35 mm cryostat tail, and the field is to be oriented in the direction perpendicular to the cryostat axis.

A good compromise among these goals was achieved by using an array of 8 cubic N52 grade NdFeB magnets positioned closely around the air gap on the perimeter of a slightly rounded square and oriented to approximate the Halbach cylinder geometry, as indicated by arrows in Fig.1(a). In contrast to the trapezoidal or arc segment magnets envisioned as the ideal implementation for Halbach cylinders [7,12], cubic rare-earth magnets are widely accessible and cost-effective, while still providing a close approximation for the Halbach cylinder magnet geometry that produced a highly uniform field as verified by simulations [Fig.1(b)] and by testing discussed below. The symmetry of the arrangement guarantees that the normal component of the field exactly vanishes on the axis of the array for any position along the axis and is negligible compared to the in-plane field for several mm deviations from the axis.

Two competing factors must be considered when optimizing the maximum achievable magnetic field magnitude: i) The magnets should be placed as close to the central axis as possible, and ii) The magnets should be as large as possible. The maximum size of the magnets is limited by the size of the air gap. Thus, we find that the cubic magnets should be of comparable size to the air gap. Using rectangular magnets with the longer dimension along the gap axis or stacking two or more identical arrangements shown in Fig.1 on top of one another can be used to increase the maximum achievable field.

The regime in which magnet sizes are comparable to the air gap is at the transition between the near-field regime, in which the dependence of the field on the distance r to the magnet center is weak and the field starts to decrease when approaching the surface of the magnet, and the dipolar regime in which the field decreases as $1/r^3$. This regime is advantageous for achieving a large almost uniform field in the gap while satisfying the geometric constraints on the possible arrangement of cubic magnets. For the desired circular gap of 36 mm, this was achieved by using 25 mm x 25 mm x 25 mm magnetic cubes. Magnets 5- 8 are symmetrically placed as close as possible to the air gap, and magnets 1-4 were then slotted in the remaining space while maintaining the symmetry. To ensure mechanical stability, the magnets are separated from the air gap by the partitions that are 1.4 mm-wide at their narrowest point, and from each other by 2.4 mm-wide partitions cut out in the aluminum carrier block to which they are glued by epoxy. In principle, partitions can be eliminated, and larger magnets can be used to achieve higher fields, but this makes the assembly of the array significantly more challenging due to the large torques exerted by the magnets on each other.

The assembly of the array required a certain order and auxiliary design elements to minimize torques and facilitate magnet insertion. The order of the assembly is labeled with numbers 1-8 in Fig.1(a). Magnets 1-4 on the diagonals were inserted first as they are widely spaced and their mutual forces and torques are modest. The torques on magnet #5 from magnets 1 and 3 are compensated as long as it is not shifted from its position in the center, so its insertion was also straightforward. Guiding slots visible in Fig.1(a) were used to insert the remaining magnets 6-8. A lid was placed on top of the array, turning these slots into channels. The magnets were inserted into the open ends of the channels and pushed in using a C-clamp. Each magnet and its mating surfaces were covered with epoxy before insertion, and the next magnet was inserted only after the epoxy had been set.

To vary the magnetic field, the aluminum carrier block is translated along the air gap axis using three lead screws driven by the stepper motor via the common 8 mm timing belt and pulley system [Fig.2(a)]. The total travel was set to 110 mm, so that in the furthest position the array produced a field of about 1.5 mT. This field was compensated to the precision of about 0.01 mT, comparable to the earth's field, by two fixed auxiliary magnets placed next to the sample position on the sides, as shown in Fig.2(a). To provide field rotation and reversal capabilities, the assembly is placed on a rotary stage driven by a separate stepper motor (not visible in Fig.2(a)). The total cost of all the components excluding the rotary stage was about $600, an order of magnitude less than a commercial electromagnet -based setup that can achieve comparable fields. The estimated cost of a rotating stage is less than $1,000 (see for example ThorLabs PRMTZ8). To estimate how effective our solution is in terms of cost and energy consumption, we compare it with consumer

electromagnets. To achieve magnetic fields of the order of 0.5 T in such a large 35 mm air gap requires a power of the order of 600 W. Depending on the model, typical electromagnets require about 0.2-0.5 W per Gauss, with a normalized cost of an electromagnet with an energy source of about $3-6 per Gauss. The power consumption of our system is negligible, and the normalized cost is about $0.3-0.6 per Gauss, depending on the cost of the rotation stage, that is, approximately an order of magnitude less. Electromagnets remain unrivaled in applications requiring magnetic fields greater than 0.5 T.

To assess the stability of the system with respect to the changes in the external environment, such as the influence of vibrations, temperature fluctuations, etc., the magnetic field was measured for 60 hours; the corresponding Allan stability plot is shown in Fig. 2(b).

III. Modeling

Finite-element numerical simulations were performed using CST Studio Suite software [14]. The N52 magnet B(H) curves were acquired from K&J Magnetics [15].

Since the faces of the magnets are in immediate proximity to the edges of the airgap, dipole approximation is not valid near the edges, but it was found to provide good agreement with the simulation results for the field close to the axis of the airgap, as shown in the next section. Such analytical calculations provide valuable insight into the relation between design parameters and the generated magnetic fields. For the nth magnet, the field was determined according to

$$\boldsymbol{B}_n(\boldsymbol{r}) = \frac{\mu_0}{4\pi}\frac{1}{(\boldsymbol{r}-\boldsymbol{r}_n)^5}\left[3\big(\boldsymbol{m}_n\cdot(\boldsymbol{r}-\boldsymbol{r}_n)\big)(\boldsymbol{r}-\boldsymbol{r}_n)-(\boldsymbol{r}-\boldsymbol{r}_n)^2\boldsymbol{m}_n\right] \quad (1)$$

where μ_0 is the vacuum permeability, $\boldsymbol{m}_n$ is the magnetic moment of the nth cube, and $\boldsymbol{r}_n$ is the position of its center. The field of the array was determined as a superposition of the fields produced by each magnet,

$$\boldsymbol{B}_{tot}(\boldsymbol{r}) = \sum_n \boldsymbol{B}_n(\boldsymbol{r}) \quad (2)$$

neglecting their mutual demagnetizing effects. The resulting expression for **B** is generally cumbersome but simplifies in special cases. We use the coordinate system with the z-axis along the cylindrical airgap and the x-axis in the intended direction of the field, and the origin **r** = (0, 0, 0) at the center of the array. For **r** = (0, 0, z) on the axis, the magnetic field takes the form

$$\boldsymbol{B} = \frac{3\mu_0 m}{2\pi}\left(\frac{a^2}{(a^2+z^2)^{5/2}}+\frac{b^2}{(b^2+z^2)^{5/2}},0,0\right), \quad (3)$$

where m=|$\boldsymbol{m}_n$|, *a (b)* is the distance to the centers of the magnets #5-8 (1-4) from the origin. In our design a=32 mm and b=39 mm, but least-squares fitting gives a=36.7 mm and b=33.9 mm, which can be

attributed to manufacturing imperfections and demagnetization effects, not included in the dipole approximation. At the origin, this expression becomes

$$\boldsymbol{B}(\boldsymbol{r}=0)=\frac{3\mu_0 m}{2\pi}\left(\frac{1}{a^3}+\frac{1}{b^3},0,0\right). \quad (4)$$

According to Eqs. (3), (4) the contribution of the four diagonal magnets to the maximum field at r=0 is almost half as large as that from the four on-axis magnets #5-8, but this difference is reduced at finite z, resulting in a more gradual dependence B(z) that would be attained with only four "on-axis" magnets, which is beneficial for field uniformity.

The properties of the magnet materials can be characterized by the flux density $B_r=\mu_0 m/V$, where V is the volume of each permanent magnet. For the N52-grade NdFeB magnets, B_r=1.48T is expected. However, we found that both CST Studio simulations and the dipole approximation overestimate the magnetic field by a factor of 1.3, while providing a good fit to the experimental data if Br=1.01T is used instead. Since this issue is not limited to dipole approximation but also persists in CST simulations, which include demagnetization effects, we attribute this discrepancy to the quality limitations of the consumer-grade cube magnets used in our setup.

For a dense pack of cubic magnets, the volume of an air gap is equal to the volume of an individual magnet with the distance between the origin and side equal to the cube side length, leading to $V=a^3=\left(\frac{b}{\sqrt{2}}\right)^3$; a magnetic field in the middle of the gap equals to $\frac{3(4+\sqrt{2})}{8\pi}B_r$, and does not depend on the size of the magnets, therefore smaller magnets can be used if a large gap is not required.

IV. Testing and experimental verification

To characterize the field produced by the setup, three separate series of measurements were performed as a function of position along the x-, y-, and z-axes, with the Hall probe oriented in the x-direction. The field dependence on the position z along the axis is shown in Fig. 3(a). As expected, the measured field is maximized at z=0 and decreases to a few mT at z=±0.11 m. The measured dependence is in excellent agreement with the calculation based on the dipole approximation [curve in Fig. 3] using B_r=1.01T. The field calculated using Br=1.48T or simulated in CST Studio Suite [open symbols in Fig.3] using B(H) curve [15] with B(H=0)=1.438T follow the same functional dependence but overestimates the experimental data, reaching a maximum value of 0.51 T instead of the experimentally observed 0.38 T.

The decay of the field with z is required for the ability to adjust its value, which necessarily compromises its uniformity along the z-direction. Nevertheless, we find that the maximum field at z=0 is

highly uniform. Near this point, the field deviates from the average by 3% within a 5 mm distance from the origin along z-axis, and by 9% within a 10 mm distance from the origin. Similarly, at large z the field becomes small and does not significantly vary with position. The maximum relative non-uniformity is reached at intermediate positions z=±1.5 cm, as can be seen from the magnetic field gradient shown as an inset in Figure 3(a).

For the displacements in x- and y- directions, the uniformity of the field increases with increasing magnitude of z, so we limit the discussion to the most inhomogeneous distribution at z=0. Figure 3(b) shows the dependence on the displacement along the x-axis, in the direction of the field. The field is minimized at the center of the air gap, increasing near the edges. At small |x|, the dependence is approximately parabolic and is in good agreement with the dipolar approximation, as shown by the curve. The dipolar approximation becomes inadequate close to the edges of the air gap, overestimating the field variation. The measured dependence flattens out, which is captured by the numeric simulation. The magnitude of the field remains within 4% of its average value for up to 7 mm distance from the center.

The dependence on the y-position transverse to the field is shown in Fig.3(c). The field is minimized at the center and increases towards the edges, qualitatively similar to the x-direction, but the dependence on y is significantly weaker than on x, remaining almost completely flat at |y|<10 mm, which is well described by the dipolar approximation. The deviation from the average is less than 0.5% within 5 mm from the center and 4% for up to 16 mm from the center. Based on these tests, we conclude that relative field uniformity of at least 2% is achieved within a volume with a 4 mm radius over the entire operational range. In nanoscience research focused on micrometer- or nanometer-scale samples, these field non-uniformity effects become negligible.

Electromagnets generally exhibit hysteresis dependence of magnetic field produced at a given driving current on their history, due to the reorientation of magnetic domains in their poles. This effect, also known as the magnetic memory, is a significant issue that in precision experiments is addressed using Hall sensor-based feedback loops. The latter can result in field overshoot, which is problematic for measurements of very narrow hysteresis loops such as those in marginally thermally stable, i.e. almost superparamagnetic systems. In the presented design, this issue is avoided altogether, since the magnitude of the magnetic field is determined by the precisely controlled position of the array. We confirm this benefit of our variable field source by anomalous Hall effect (AHE) measurements on a magnetic thin-film heterostructure Ti(1.5)Pt(2)$Co_{40}Fe_{40}B_{20}$(0.4)AlO_x(2), where thicknesses are in nanometers. While the bulk CoFeB is ferromagnetic at room temperature and is expected to exhibit a hysteretic dependence of AHE on the field,

because of the confinement effects the Curie point of ultrathin $Co_{40}Fe_{40}B_{20}$ layer in this sample is expected to be in the vicinity of room temperature, and thus it is not expected to exhibit any hysteresis in the field-dependence. Indeed, room-temperature measurement [Fig.4] shows a nonlinear dependence of the Hall voltage on the field expected due to the nonlinear susceptibility close to the Curie point, but hysteresis is completely absent in this measurement, as is evident from the zoom-in on small-field values in panel (b) of Fig.4.

V. Summary

We have developed a simple-to-implement, compact, and robust variable magnetic field source based on an array of rare-earth permanent magnet cubes approximating a Halbach cylinder. The maximum theoretical field achieved for the air gap of 36 mm is 0.5T, substantially exceeding the capabilities of compact electromagnets such as GMW 3470 widely used in small-scale laboratory research, at an order of magnitude smaller cost. The actual maximum field of 0.38 T determined in our testing is somewhat smaller, likely due to the consumer-grade quality of magnets used in our setup. The variation of the field is produced by the axial motion of the array, which results in a modest field inhomogeneity of only up to 2% over the 4 mm radius, and 4% over the 7 mm radius at intermediate fields, representing a reasonable compromise for typical sample sizes used in science research and development.

Among the many advantages of the presented source is high field stability and negligible remanence without the need for the feedback loop which can be eliminated by an anti-backlash mechanism, allowing one to reproducibly obtain precise values of small fields for highly sensitive experiments, such as high-precision optical measurements of atomic emission spectra. The presented approach may be suitable for the development of efficient quantum computers based on superconducting qubits or trapped ions [10,16].

Acknowledgments

This work was supported by the NSF award ECCS-2005786.

Data availability

The data that support the findings of this study are available from the corresponding author upon reasonable request.

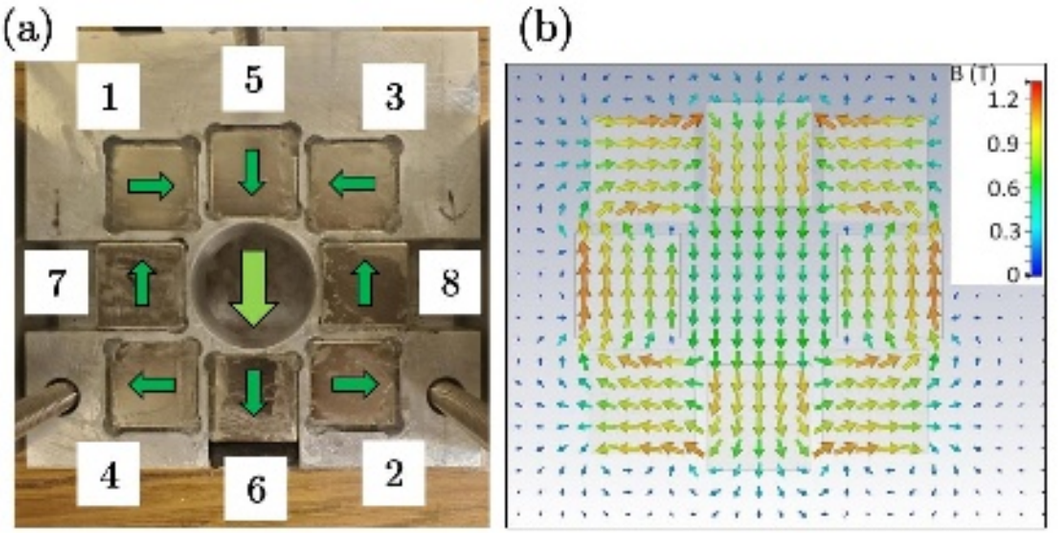

Fig.1. (a). Photograph of the Halbach array used to generate a dipole magnetic field. Arrows show the directions of cube magnet magnetization, numbers show the assembly sequence. (b) Calculated magnetic field distribution in the array plane.

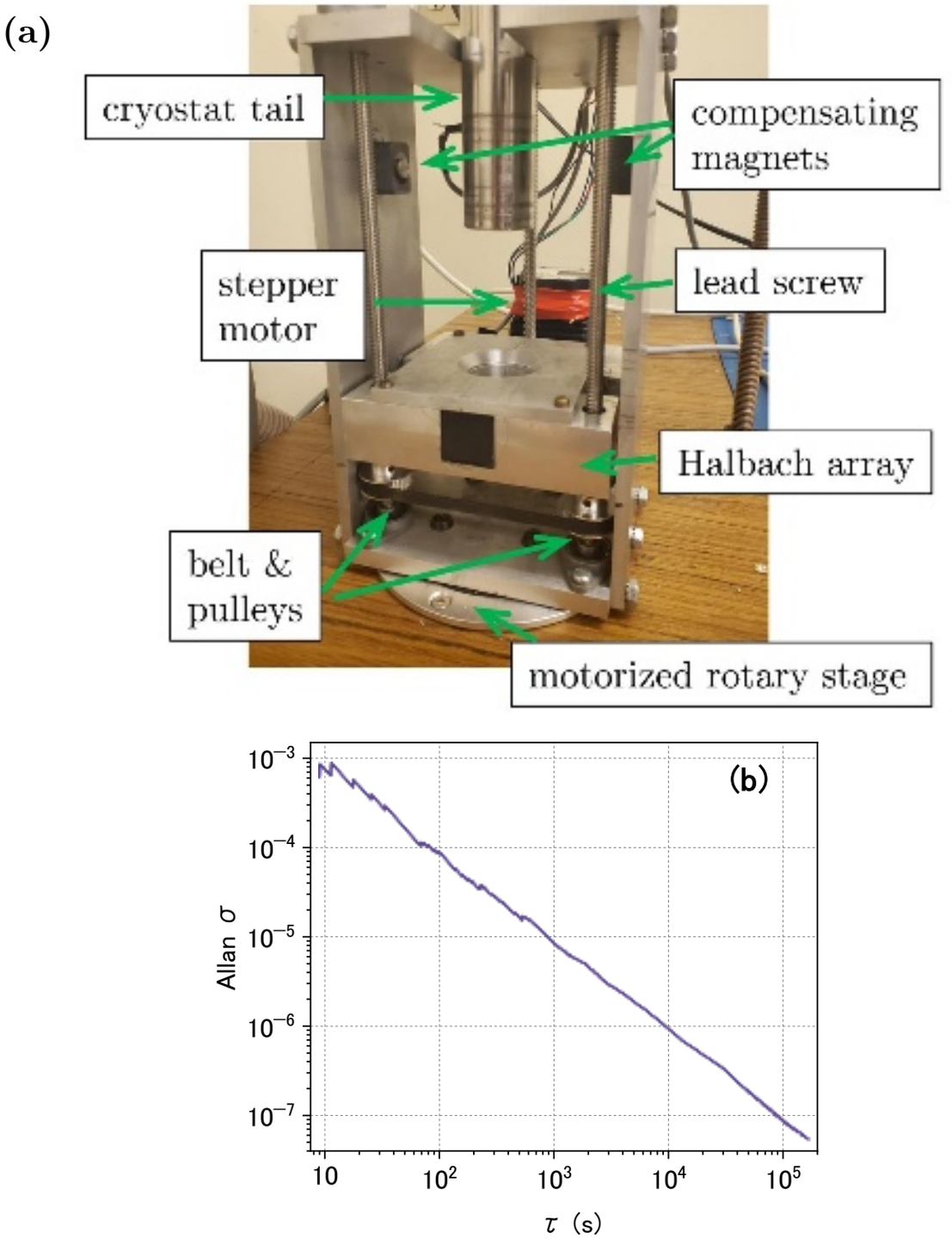

Fig.2. (a) Photograph of the assembly including the stages for the array translation and rotation, (b) Allan stability plot.

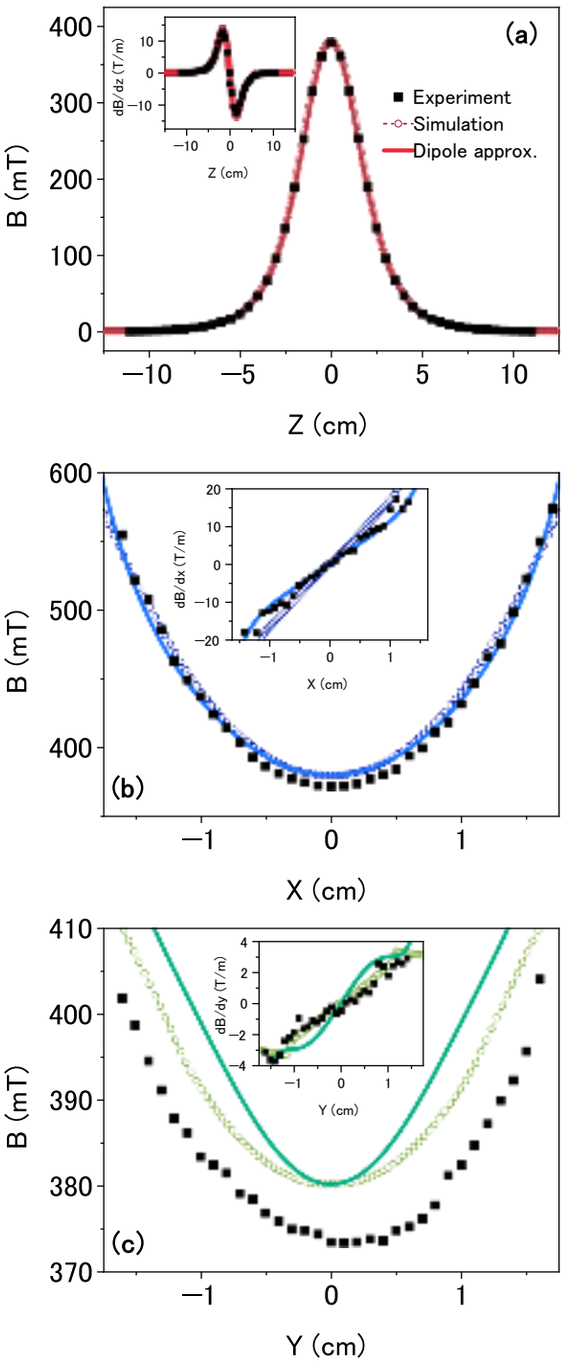

Fig.3. (a)-(c) Dependence of field on the displacement from the center of the array in the z-direction (a), the x-direction (b), and the y-direction (c). Solid symbols: measured values, curves: dipolar approximation, open symbols: finite-element simulation, scaled down by a factor of 1.3, as described in the text. Insets: gradient of the magnetic field.

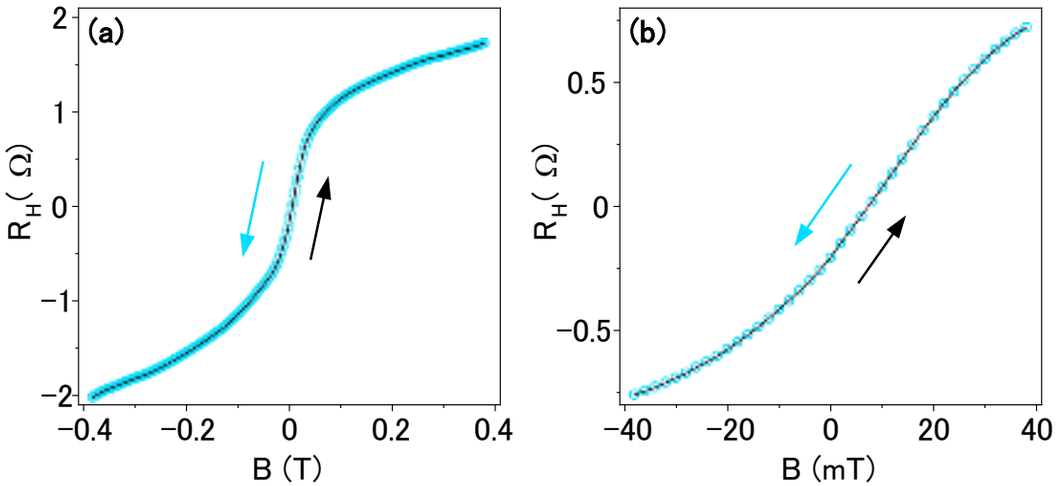

Fig.4. (a) Anomalous Hall effect hysteresis loop for a Ti(1.5)Pt(2)CoFeB(0.4)AlO_x(2) sample. (b) Zoom in on the small-field range of the same loop showing negligible hysteresis. The data are offset to compensate for the accidental asymmetry of the Hall contacts. The magnetic field was changed by moving the magnetic array along the Z axis and rotating around the Z axis to change the magnetic field polarity.

References

[1] C. Windt, H. Soltner, D. van Dusschoten, and Peter Blümler, A portable Halbach magnet that can be opened and closed without force: The NMR-CUFF, *Journal of Magnetic Resonance*, 208 (1): 27–33 (2011).

[2] J.M.D. Coey, Permanent magnet applications, *Journal of Magnetism and Magnetic Materials*, 248 (3): 441–456 (2002).

[3] Jae-Seok Choi and Jeonghoon Yoo, Design of a Halbach Magnet Array Based on Optimization Techniques, *IEEE Transactions on Magnetics*, 44 (10): 2361–2366 (2008)

[4] G. Herzer, Modern soft magnets: Amorphous and nanocrystalline materials, *Acta Materialia*, 61 (3): 718–734 (2013).

[5] J.C. Mallinson "One-Sided Fluxes — A Magnetic Curiosity?". *IEEE Transactions on Magnetics*. 9 (4): 678–682 (1973).

[6] K. Halbach, "Design of permanent multipole magnets with oriented rare earth cobalt material". *Nuclear Instruments and Methods*. **169** (1): 1–10 (1980).

[7] K. Halbach "Applications of Permanent Magnets in Accelerators and Electron Storage Rings", *Journal of Applied Physics*. **57** (1): 3605–3608 (1985).

[8] M. Kumada, E.I. Antokhin, Y. Iwashita M. Aoki and E. Sugiyama "Super Strong Permanent Magnet Quadrupole for a Linear Collider" *IEEE Transactions on Applied Superconductivity*. **14** (2): 1287–1289 (2004).

[9] A. Sarwar; A. Nemirovski; B. Shapiro "Optimal Halbach permanent magnet designs for maximally pulling and pushing nanoparticles" (PDF). *Journal of Magnetism and Magnetic Materials*. **324** (5): 742–754 (2012)

[10] C. Adambukulam, V. K. Sewani, H. G. Stemp, S. Asaad, M. T. Mądzik, A. Morello, A. Laucht; An ultra-stable 1.5 T permanent magnet assembly for qubit experiments at cryogenic temperatures. *Rev. Sci. Instrum.* 92 (8): 085106 (2021).

[11] F. Bloch, O. Cugat, G. Meunier, and J.C. Toussaint "Innovating approaches to the generation of intense magnetic fields: design and optimization of a 4 Tesla permanent magnet flux source". *IEEE Transactions on Magnetics*. **34** (5): 2465–2468 (1998).

[12] T. R. Ni Mhiochain; D. Weaire; S. M. McMurry; J. M. D. Coey "Analysis of torque in nested magnetic cylinders". *Journal of Applied Physics*. **86** (11): 6412–6424 (1999).

[13] R. Bjørk; A. Smith; C. R. H. Bahl "Analysis of the magnetic field, force, and torque for two-dimensional Halbach cylinders", *Journal of Magnetism and Magnetic Materials*. **322** (1): 133–141 (2010).

[14] CST STUDIO SUITE 2023, Dassault Systèmes Simulia Corp., https://www.cst.com

[15] K&J Magnetics Inc., https://www.kjmagnetics.com

[16] D. Kielpinski, C. Monroe, D.J. Wineland "Architecture for a large-scale ion-trap quantum computer" *Nature*. **417** (6890): 709–711 (2002)